Excited states by quantum Monte Carlo methods: Imaginary time evolution with projection operators

D. Blume,[1,2] M. Lewerenz,[1] P. Niyaz,[2] and K. B. Whaley[1,2]
[1]*Max-Planck-Institut für Strömungsforschung, Bunsenstrasse 10, D-37073 Göttingen, Germany*
[2]*Department of Chemistry, University of California, Berkeley, California 94720*
(Received 15 November 1996)

We present a Monte Carlo algorithm suitable for the calculation of excited state energies of multidimensional quantum systems. Energies are extracted from a maximum entropy analysis of the imaginary time evolution of a state prepared by application of a projection operator on an initial wave function. The imaginary time evolution is computed with a pure diffusion Monte Carlo algorithm. The method is demonstrated on a harmonic oscillator and several Morse oscillator test problems. [S1063-651X(97)07503-X]

PACS number(s): 02.70.Lq, 02.50.Wp, 33.20.Tp, 36.20.Ng

I. INTRODUCTION

Excited states play a central role in the physics and chemistry of atoms, molecules, and clusters. Despite many efforts, however, the exact theoretical description of the complete vibrational spectrum of a system with many degrees of freedom in the general case of anharmonic potential surfaces and large amplitude motions has remained elusive. Normal mode descriptions that can easily handle several hundred degrees of freedom are applicable only to vibrational motions in large molecules with stiff bonds and small atomic displacements. Variational basis set expansions that do not make any approximations to the Hamiltonian have remained restricted to small molecules with currently up to six degrees of freedom [1,2] because of the computational complexity of the problem, although they can in principle provide a large number of energy levels and corresponding wave functions.

Complementary in many ways to the exact variational methods developed for small systems are the stochastic approaches collectively referred to as quantum Monte Carlo methods. These methods are ideal tools for the study of the vibrational ground state of very large systems [3–6] or the determination of thermodynamic properties of quantum systems [7,8]. They have reached a very high degree of sophistication in recent years. The extraction of information on excited states from this type of calculation has, however, proven to be very difficult.

Successful adiabatic extensions of the diffusion quantum Monte Carlo (DMC) method have been designed for specific problems [6,9–12]. Special methods exist for cases with known nodal surfaces [9,10,13–16]. Both approaches, however, do not provide a general solution to the problem. Early attempts at successive orthogonalization [17] have remained restricted to few degrees of freedom. Several efforts aiming at an automatic construction of nodal surfaces [18–20] have been published recently. A promising technique that has been demonstrated to date on relatively small problems is the correlation function quantum Monte Carlo (CFMC) approach initiated by Ceperley *et al.* [21–23].

Another class of methods has been designed based on the fact that finite temperature thermodynamic data and correlation functions in principle contain information on the complete set of bound states of any many-body system. These properties can be relatively easily computed with the path integral Monte Carlo (PIMC) technique. Most of the efforts in this class were directed towards the calculation of the real time dynamics of quantum systems [24–30], which requires knowledge of the complete spectrum [31–33]. The biggest obstacle in the practical application of these latter approaches is the extraction of a spectral density, which is similar to performing an inverse Laplace transform numerically. This is a well known ill-posed problem.

The numerical solution of the inverse Laplace transform problem has been attempted in the past with least-squares approaches [31] and various regularization methods [34–38]. Among these techniques the regularized inverse Laplace transform using Padé approximations [34,39] and the method of Brianzi *et al.* [37,38] appear attractive. For the present problem of strongly structured spectra the implicit smoothness assumptions of these methods turned out to be unsuitable, however. In practice, the maximum entropy method (MEM) has proven to date to be the most powerful tool for the solution of this inverse problem, and has found a high degree of popularity [26,32,33,40,41]. A combination of finite temperature PIMC and maximum entropy data analysis has been used successfully for the description of electron bubbles in helium [33] and oscillator chains [41]. A problem observed in several of these applications is the increasing difficulty to provide a reliable data analysis if several peaks are present in the target spectrum. This situation becomes worse with increasing number of degrees of freedom, since the finite temperature data always include all energy levels of the system under investigation.

The method proposed in this paper was inspired by a similar approach of Carlson and Schiavilla who used Green's function Monte Carlo (GFMC) to calculate the Euclidean proton response [42]. Our approach extracts excited state energies from a maximum entropy analysis of the imaginary time evolution of an initial state. The imaginary time evolution is computed with a zero temperature diffusion Monte Carlo algorithm. Application of an additional projector on the initial wave function allows us to restrict the number of peaks in the spectrum. One can therefore construct the complete spectrum by the application of a sequence of projectors.

However, for many of the applications which we are aiming at, complete knowledge of the spectrum is not even required. For example, if the goal of our calculation is the estimation of the optical excitation spectrum of a molecule embedded into a matrix or a cluster [4,6], we can tailor the projector to selectively suppress the collective excitations of the matrix in order to gain information on the matrix shift of the molecule or to extract exclusively information on collective excitations accompanying molecular excitations in the form of phonon side bands. A particularly interesting observation of the latter phenomenon has been made in electronic excitation spectra of molecules embedded into large liquid helium clusters [43]. For such a spectroscopic application the projection operator can be, e.g., identified with the dipole operator. However, we note that our method shares with the finite temperature versions the limitation to the calculation of energies only. The determination of transition matrix elements and other properties of excited states remains beyond the scope of the method.

The organization of the paper is as follows: Section II presents the essential features of our quantum Monte Carlo method and gives details on the implementation of the algorithm. The maximum entropy method employed for the data analysis is summarized in Sec. III. Section IV discusses applications to several one-dimensional oscillator test problems of increasing complexity (harmonic oscillator, Morse oscillators with increasing anharmonicity), which illustrate both the scope of the method and the effect of the choice of different projectors. Section V summarizes the results and gives an outlook on future applications to realistic molecular cluster systems.

II. THE QUANTUM MONTE CARLO METHODS

A. General formalism

The wave function of a system, $\Psi(R,t)$, can be formally written in an eigenfunction expansion [15],

$$\Psi(R,t)=\sum_{j=0}^{\infty} c_j\psi_j(R)\exp\left[-(E_j-E_{\rm ref})\frac{t}{\hbar}\right], \tag{1}$$

where t is an imaginary time, $E_{\rm ref}$ is an arbitrary energy shift, and E_j and ψ_j are the eigenenergies and eigenstates of the system,

$$H|\psi_j\rangle=E_j|\psi_j\rangle. \tag{2}$$

For sufficiently large t, only the lowest eigenstate, ψ_0, contributes to Ψ. The standard DMC algorithm exploits this property to project out the stationary ground state wave function using the time-dependent Schrödinger equation. Contributions from higher excited states decay fast in comparison to contributions from lower excited states. Properties of the stationary ground state, ψ_0, like the energy expectation value can be calculated after the decay process is complete [3].

It is evident from Eq. (1) that the imaginary time dependence of the Monte Carlo solution during the decay phase, which is usually discarded in DMC calculations, contains information about the complete energy spectrum, $E_j-E_{\rm ref}$. The expectation value of the quantity

$$I(t)=\langle\psi_T|\exp\left[-(H-E_{\rm ref})\frac{t}{\hbar}\right]|\psi_T\rangle \tag{3}$$

can be sampled from a DMC random walk by evaluating

$$I(t)=\langle W(t)\rangle, \tag{4}$$

where W is the cumulative branching weight used in pure DMC,

$$W(t)=\prod_{k=0}^{N}\exp\left[-(E_L(R_k)-E_{\rm ref})\frac{\Delta t}{\hbar}\right], \tag{5}$$

and the angular brackets denote a statistical average [3]. The R_k denote positions in configuration space and are distributed with the density $|\psi_T|^2$. ψ_T is a trial wave function, and E_L is the local energy, $E_L=\psi_T^{-1}H\psi_T$. One normally takes $E_{\rm ref}$ close to E_T for efficiency, where E_T is defined by $E_T=\langle\psi_T|H|\psi_T\rangle/\langle\psi_T|\psi_T\rangle$. Δt is the DMC time step; the imaginary time t is divided into a large number of small time steps, Δt.

The exponential energy dependence of Eq. (4) presents serious problems, especially when the noise of the Monte Carlo simulation is non-negligible and when we have to deal with multi exponential decays. A more sophisticated approach derives from writing $I(t)$ in an integral representation [40],

$$I(t)=\int_{-\infty}^{\infty}\sum_{j=0}^{\infty}\delta(E-E_j+E_{\rm ref})\langle\psi_T|\psi_j\rangle^2\exp(-tE)dE. \tag{6}$$

The E_j may then be extracted from $I(t)$ by performing the inverse Laplace transform, which is, however, a known ill-conditioned numerical problem. Our approach is based on Eq. (3) and Eq. (6), but includes an additional projection operator A, which allows the sequential extraction of excited energies. Then the inverse Laplace transform is still an ill-posed problem but the resulting exponential decay is dominated by only a few eigenenergies, rather than by many eigenenergies simultaneously.

Our derivation starts with a rate expression, $\kappa(\omega)$,

$$\kappa(\omega)=\sum_f|\langle\psi_i|A|\psi_f\rangle|^2\delta(E_i-E_f+\hbar\omega), \tag{7}$$

where ψ_i and ψ_f are the initial and final eigenstates of the system having energies E_i and E_f, respectively. We will see later that A really acts as a projector. Equation (7) simplifies, e.g., to Fermi's golden rule expression if we identify the projection operator A with a coupling potential V and include appropriate prefactors. Then we have an expression for the linewidth, $\Gamma(\omega)$. McMahon and Whaley [44] have used this modified formula to calculate energy transfer rates in doped quantum clusters.

Our first step is to take the Laplace transform of Eq. (7),

$$\mathcal{L}\{\kappa(\omega)\}=\tilde{\kappa}(t)=\int_0^{\infty}\left[\sum_f|\langle\psi_i|A|\psi_f\rangle^2|\times\delta(E_i-E_f+\hbar\omega)\right]\exp(-\omega t)d\omega \tag{8a}$$

$$= 1/\hbar \sum_f |\langle \psi_i|A|\psi_f\rangle|^2 \exp\left[-(E_f - E_i)\frac{t}{\hbar}\right]. \tag{8b}$$

The form of Eq. (8b) suggests that we identify t as an imaginary time. We now relate this to the imaginary time propagation of the DMC method. Rewriting Eq. (8b) as

$$\tilde{\kappa}(t) = 1/\hbar \sum_f \langle \psi_i|A|\psi_f\rangle \exp\left[-(E_f - E_i)\frac{t}{\hbar}\right] \langle \psi_f|A^+|\psi_i\rangle \tag{9}$$

and moving the exponential of $E_f t/\hbar$ to the left yields

$$\tilde{\kappa}(t) = 1/\hbar \sum_f \langle \psi_i|A \exp\left[-(H - E_i)\frac{t}{\hbar}\right] |\psi_f\rangle \langle \psi_f|A^+|\psi_i\rangle, \tag{10}$$

where H is the Hamiltonian of our system,

$$H|\psi_f\rangle = E_f|\psi_f\rangle. \tag{11}$$

Using closure to remove the sum over final states then results in

$$\tilde{\kappa}(t) = 1/\hbar \langle \psi_i|A \exp\left[-(H - E_i)\frac{t}{\hbar}\right] A^+|\psi_i\rangle. \tag{12}$$

Thus we have employed the imaginary time Laplace transform in order to introduce the correspondence with a DMC propagation: see Eq. (3). Equation (12) is identical with Eq. (3) for $A = 1$. The crucial advantage of Eq. (12) in comparison to Eq. (3) is that we are able to choose an arbitrary projection operator A, which projects on different wave functions. As stated earlier, this allows us to extract energy differences sequentially by using a sequence of suitable projection operators.

With Eq. (12) we now have an expression for energy differences involving a matrix element evaluated over only the initial state. This matrix element can be evaluated using a multidimensional Monte Carlo integration for the $t = 0$ component and a DMC walk, which propagates $A^+|\psi_i\rangle$, according to $\exp[-(H - E_i)t/\hbar]$. Each configuration used for the calculation of the multidimensional integral is propagated by such a DMC walk. This scheme is reminiscent of the ''sidewalk algorithm'' developed for the calculation of exact expectation values by quantum Monte Carlo [45]. However, it should be mentioned that our implementation is a ''pure'' DMC method, which allows the usual exponential growth and decay but no branching or annihilation of DMC random walkers. The latter is introduced in most DMC algorithms in order to increase the computational efficiency. However, here we are interested in the decay of the weights as a function of imaginary time, and therefore it is not advisable to ''artificially'' modify these. The Monte Carlo formalism for the determination of $\tilde{\kappa}(t)$ will be described in more detail in the following.

For convenience we use an unnormalized initial wave function ψ_i. Equation (12) is then rewritten with a normalization factor,

$$\tilde{\kappa}(t) = \frac{\langle \psi_i|A \exp[-(H - E_i)t/\hbar] A^+|\psi_i\rangle}{\hbar \langle \psi_i|\psi_i\rangle}. \tag{13}$$

Now we insert closure relations for R and R', where R and R' are coordinate vectors,

$$\tilde{\kappa}(t) = 1/\hbar \frac{\int dR \int dR' \langle \psi_i|A|R'\rangle \langle R'|\exp[-(H - E_i)t/\hbar]|R\rangle \langle R|A^+|\psi_i\rangle}{\langle \psi_i|\psi_i\rangle} \tag{14a}$$

$$= 1/\hbar \frac{\int dR \int dR' \psi_i(R) A^+(R) \langle R'|\exp[-(H - E_i)t/\hbar]|R\rangle A(R') \psi_i(R')}{\int dR'' \psi_i^2(R'')}. \tag{14b}$$

Multiplying the integral by $\psi_i(R)\psi_i^{-1}(R) = 1$, and recognizing that

$$G(R', R, t) = \langle R'|\exp\left[-(H - E_i)\frac{t}{\hbar}\right]|R\rangle \tag{15}$$

is the usual Green's function, leads to

$$\tilde{\kappa}(t) = 1/\hbar \int dR \frac{\psi_i^2(R)}{\int dR'' \psi_i^2(R'')} A^+(R) \int dR' \psi_i^{-1}(R) G(R', R, t) \psi_i(R') A(R'). \tag{16}$$

Substituting now the importance sampling Green's function [3],

$$G_I(R', R, t) = \psi_i^{-1}(R) G(R', R, t) \psi_i(R'), \tag{17}$$

yields

$$\tilde{\kappa}(t)=1/\hbar \int dR \frac{\psi_i^2(R)}{\int dR'' \psi_i^2(R'')} A^+(R) \int dR' G_I(R',R,t) A(R'). \tag{18}$$

Equation (18) is expanded by introducing an integral over a δ function,

$$\tilde{\kappa}(t)=1/\hbar \int dR \frac{\psi_i^2(R)}{\int dR'' \psi_i^2(R'')} A^+(R) \int dR' A(R') \int dR''' G_I(R',R''',t)\,\delta(R'''-R), \tag{19}$$

which leads directly to a Monte Carlo representation. The outer integration over R can be performed via a multidimensional Monte Carlo integration, where a chain of configurations, $R_k^{(0)}$, $k=1,\ldots,p$, distributed with the density $|\psi_i|^2$, is sampled by using the Metropolis algorithm [46]. The integration over R' can be realized by a DMC walk that propagates each initial configuration $R_k^{(0)}$ in imaginary time, where the upper index (0) refers to the imaginary time, $t=0$. The propagated configurations, R_k' will be labeled for notational simplicity by $R_k^{(t)}$. With this in hand we can formulate the Monte Carlo representation of Eq. (19),

$$\tilde{\kappa}(t)=\frac{1}{\hbar p} \sum_{k=1}^{p} A^+(R_k^{(0)}) A(R_k^{(t)}) w(R_k^{(t)},\Delta t), \tag{20}$$

where $w(R_k^{(t)},\Delta t)$ is the weight of the DMC random walker at $R_k^{(t)}$ at time t [47]. The weight $w(R_k^{(t)},\Delta t)$ depends on the initial configuration $R_k^{(0)}$, on the instantaneous DMC configuration $R_k^{(t)}$, and on the finite DMC time step Δt. Now we have an explicit expression for evaluating Eq. (13) through a combination of a multidimensional Monte Carlo integration with DMC walks linked to each sampling point.

Since the initial wave function ψ_i has to be nodeless in order to perform the suggested Monte Carlo algorithm as outlined above, we should use the ground state wave function ψ_0 as the initial wave function ψ_i. In general, however, we do not know the exact ground state wave function and energy. Therefore we use a trial wave function ψ_T, which should approximate the exact ground state wave function ψ_0 as closely as possible. Additionally we normally employ a reference energy $E_{\rm ref}$ instead of the exact ground state energy E_0. $E_{\rm ref}$ should be close to E_0 and a popular and efficient choice in DMC calculations is $E_{\rm ref}=E_T$. Thus, in practice Eq. (13) would give us energies relative to the reference energy $E_{\rm ref}$. In order to remove any such dependence of $\kappa(\omega)$ on $E_{\rm ref}$, we incorporate an additional normalization factor. This leads to the expression

$$\tilde{\kappa}(t)=\frac{\dfrac{\langle \psi_T | A \exp[-(H-E_{\rm ref})t/\hbar] A^+ | \psi_T \rangle}{\langle \psi_T | \psi_T \rangle}}{\dfrac{\langle \psi_T | \exp[-(H-E_{\rm ref})t/\hbar] | \psi_T \rangle}{\langle \psi_T | \psi_T \rangle}} \tag{21a}$$

$$=\frac{(1/p)\sum_{k=1}^{p} A^+(R_k^{(0)}) A(R_k^{(t)}) w(R_k^{(t)},\Delta t)}{(1/p)\sum_{k=1}^{p} w(R_k^{(t)},\Delta t)}, \tag{21b}$$

which can easily be shown to exhibit the required independence of the imaginary time signal on both the choice of the reference energy, $E_{\rm ref}$, and the scaling of the weights of the random walkers. The initial configurations $R_k^{(0)}$ are now sampled from $|\psi_T(R)|^2$. This normalization is identical to that suggested by Carlson and Schiavilla [42], although theirs was not motivated by the same consideration.

In principle, employing ψ_T rather than ψ_0 introduces a systematic error. This can be analyzed by performing the inverse Laplace transform of Eq. (21a). The transform of Eq. (21a) can be done analytically if we write the trial wave function in an expansion in the exact eigenstates. The trial wave function has to be close enough to the ground state wave function to ensure that the coefficient of the ground state wave function is at least $\sqrt{0.5}$. In this situation we can expand each component of the expansion in a series and perform the inverse Laplace transform for each term of the series. The zeroth order term of the resulting expression for $\kappa(\omega)$ is identical with the inverse Laplace transform of Eq. (13), apart from a scale factor. The higher order contributions result in additional peaks in the spectrum: these have highly reduced intensity in comparison to the intensity of the peaks resulting from the zeroth order contribution. Thus the additional normalization factor introduced in Eq. (21) provides the independence of the final expression from the reference energy but does not change the relevant features of the resulting spectrum. We demonstrate the influence of a trial wave function that is not equal to the exact ground state wave function in the application to the harmonic oscillator (see Sec. IV A).

B. Implementation

We have to create p initial configurations, $R_k^{(0)}$, $k=1,\ldots,p$, in order to evaluate Eq. (21b). Each initial configuration $R_k^{(0)}$ is used as the starting configuration for a DMC walk and the value of the projection operator $A(R_k^{(0)})$ is stored for each k. Since we need a large number p of initial configurations in order to calculate $\tilde{\kappa}(t)$ with high statistical accuracy we use sets of only n initial configurations, $R_k^{(0)}$, $k=1,\ldots,n$, at a time and repeat this procedure m times, where $p=nm$.

Then our algorithm to evaluate Eq. (21b) is the following. We pick a starting configuration $R_{11}^{(0)}$. Using the Metropolis algorithm [46] we create a chain of configurations $R_{11}^{(0)}, R_{12}^{(0)}, \ldots, R_{1l}^{(0)}, R_{21}^{(0)}, R_{22}^{(0)}, \ldots, R_{2l}^{(0)}, \ldots$. The maximal value l of the second lower index is chosen to be larger than the autocorrelation length of the system. We shall refer to l as the skip parameter in the following. The configura-

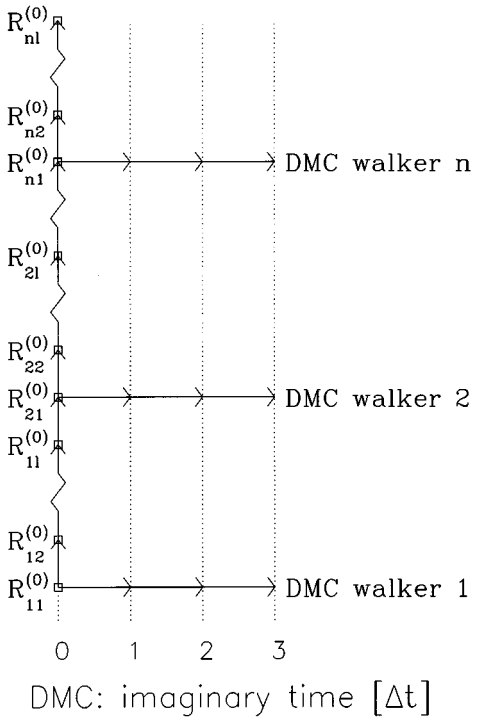

FIG. 1. Scheme for the Monte Carlo algorithm. The multidimensional Monte Carlo integration is shown schematically on the vertical axis and the DMC walk is shown schematically on the horizontal axis. The configurations $R^{(0)}_{1l},R^{(0)}_{2l},\ldots,R^{(0)}_{nl}$ are sampled from $|\psi_T(R)|^2$. l is the skip parameter used for the creation of initial configurations, $R^{(0)}_{kl}$, $k=1,\ldots,n$, and n is the number of DMC walkers. The imaginary time evolution is shown for the first three DMC time steps Δt, $2\Delta t$, and $3\Delta t$.

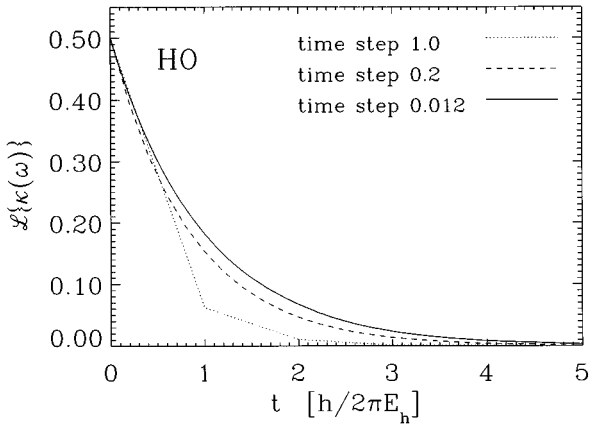

FIG. 2. Harmonic oscillator. The simulated exponential decay, $\mathcal{L}\{\kappa(\omega)\}=\tilde{\kappa}(t)$, obtained using the exact ground state wave function ψ_0 and the projector $\hat{x}$. The time steps are $\Delta t=1.0(\hbar/E_h)$, $\Delta t=0.2(\hbar/E_h)$, and $\Delta t=0.012(\hbar/E_h)$. We also performed simulations using time steps $\Delta t=0.007(\hbar/E_h)$ and $\Delta t=0.002(\hbar/E_h)$. The resulting exponential decay for these smaller values of Δt is indistinguishable from the decay with $\Delta t=0.012(\hbar/E_h)$. The time step in the legend is given in atomic units.

tions $R^{(0)}_{k1}$, $k=1,\ldots,n$, are therefore independent samples for the Monte Carlo integration and can be used as starting configurations for the DMC walk, which propagates along the imaginary time t. $A(R^{(0)}_{k1})$, $k=1,\ldots,n$ is evaluated for each k and $(1/n)\Sigma_{k=1}^{n}A(R^{(0)}_{k1})$ is stored. The vector $A(R^{(0)}_{k1})$, $k=1,\ldots,n$ is handed over to the DMC routine. The initial weights for the DMC walk are set equal to 1, but weights are updated depending on the position $R^{(t)}_{k1}$. During the DMC walk we store $(1/n)\Sigma_{k=1}^{n}w(R^{(t)}_{k1},\Delta t)$ and $(1/n)\Sigma_{k=1}^{n}w(R^{(t)}_{k1},\Delta t)A(R^{(t)}_{k1})A(R^{(0)}_{k1})$ as functions of imaginary time t. We make N DMC time steps, where the discrete DMC time step Δt has to be chosen carefully depending on the system under investigation. The accuracy of the exponential decay of the DMC weights depends strongly on the DMC time step. DMC calculations used to simulate the stationary ground state allow an extrapolation to $\Delta t=0$ from runs at several Δt since an equilibrium state is sampled. However, we are interested here in the exponential decay of the DMC weights, which are sampled from a *nonequilibrium* state. Therefore we are not able to make a time step extrapolation to $\Delta t=0$. So we have to use a time step small enough that further reduction does not change the result for $\tilde{\kappa}(t)$. The systematic time step problem is dicussed in Sec. IV A and is illustrated in Fig. 2 for the harmonic oscillator. Once the DMC propagation is finished, the results for $(1/n)\Sigma_{k=1}^{n}w(R^{(t)}_{k1},\Delta t)$ and $(1/n)\Sigma_{k=1}^{n}w(R^{(t)}_{k1},\Delta t)A(R^{(t)}_{k1})A(R^{(0)}_{k1})$ as a function of time t are returned to the multidimensional Monte Carlo integration.

Figure 1 shows a scheme for the implementation of the Monte Carlo integration and the DMC walk. This scheme shows the configurations for the first n samples of the Monte Carlo integration and n DMC walkers starting at these configurations. The calculation sketched in the scheme has to be repeated m times. The division by the correction factor of Eq. (21b) is carried out at the end of the simulation.

Now the algorithm for evaluating Eq. (21b) is given. The choice of ψ_T and A is discussed in Secs. IV and V for our particular applications. Computational parameters (e.g., DMC time step Δt, numbers for p, l, and N) are given in Secs. IV A and IV B. The next section describes the inverse Laplace transform of $\tilde{\kappa}(t)$ with MEM, in order to complete the calculation of $\kappa(\omega)$.

III. THE MAXIMUM ENTROPY ANALYSIS

The inverse Laplace transform is a well-known ill-posed numerical problem. The maximum entropy method [26,32,48,49] is based on Bayesian statistics and provides a consistent probabilistic theory to obtain unbiased results, independent of any model assumptions. A recent review by Jarrell and Gubernatis [50] gives a good introduction to Bayesian statistical inference and to the principle of maximum entropy, and also discusses some technical details. Our use of the maximum entropy method differs somewhat from the more common application to real time continuation of imaginary time data, in that we are concerned with a Laplace kernel for the inverse transform. We restrict ourselves here to a short summary of the main ideas, following Gubernatis *et al.* [26], and explain some details specific to the present applications.

Bayes's theorem relates the probability distribution function, $P[\kappa(\omega)|\tilde{\kappa}(t),I]$, to the probability distribution function $P[\kappa(\omega)|I]$, which encodes our prior knowledge,

$$P[\kappa(\omega)|\tilde{\kappa}(t),I]\propto P[\tilde{\kappa}(t)|\kappa(\omega),I]P[\kappa(\omega)|I]. \quad (22)$$

Here $P[\kappa(\omega)|\tilde{\kappa}(t),I]$ summarizes our inference about the spectral density function $\kappa(\omega)$ given the Monte Carlo data $\tilde{\kappa}(t)$ and relevant background information I such as prior knowledge about $\kappa(\omega)$. $P[\kappa(\omega)|I]$ is called the prior probability distribution and represents our state of knowledge about $\kappa(\omega)$ before we have the data. This prior state of knowledge is modified by the data through the so-called likelihood function, $P[\tilde{\kappa}(t)|\kappa(\omega),I]$, which encodes details about the nature of the Monte Carlo simulation. The product of the prior probability distribution function and the likelihood function yields the *posteriori* probability distribution function and represents our state of knowledge about $\kappa(\omega)$ after we have analyzed the data. The likelihood function, $P[\tilde{\kappa}(t)|\kappa(\omega),I]$, tells us how likely it is that we would have simulated the data we actually did, given an underlying $\kappa(\omega)$. In order to compute the likelihood function it is therefore essential to be able to calculate an ideal data set $\tilde{\kappa}_{\rm ideal}(t)$ from a given spectral density function $\kappa(\omega)$. The relevant transform is given in our case by

$$\tilde{\kappa}_{\rm ideal}(t)=\int_0^\infty d\omega\, K(t,\omega)\kappa(\omega), \quad (23)$$

with the specific kernel,

$$K(t,\omega)=\exp(-t\omega). \quad (24)$$

We make the customary assumption that the Monte Carlo data are subject to additive Gaussian noise with a root-mean-square error σ_r. Empirical tests of the data distributions discussed in the next section justify these assumptions. Then the likelihood function takes the form

$$P[\tilde{\kappa}(t)|\kappa(\omega),I]\propto\exp\left(-\frac{\chi^2}{2}\right), \quad (25)$$

where χ^2 is given by

$$\chi^2=\sum_{rs}^{N}[\tilde{\kappa}(r\Delta t)-\tilde{\kappa}_{\rm ideal}(r\Delta t)][C^{-1}]_{rs}\times[\tilde{\kappa}(s\Delta t)-\tilde{\kappa}_{\rm ideal}(s\Delta t)], \quad (26)$$

where Δt is the discrete DMC time step, N is the number of DMC time steps, and $[C^{-1}]_{rs}$ is an element of the inverse covariance matrix. C describes the correlations between the Monte Carlo data,

$$C_{rs}=\frac{\langle\tilde{\kappa}(r\Delta t)\tilde{\kappa}(s\Delta t)\rangle-\langle\tilde{\kappa}(r\Delta t)\rangle\langle\tilde{\kappa}(s\Delta t)\rangle}{M-1}, \quad (27)$$

where M is the number of independent samples of each $\tilde{\kappa}(r\Delta t)$ and the angular brackets denote a statistical average. If the errors σ_r are independent, the nondiagonal elements of the covariance matrix C are equal to zero and Eq. (26) simplifies to the usual sum-of-squared-residuals misfit statistic [51],

$$\chi^2=\sum_r^N\left[\frac{\tilde{\kappa}(r\Delta t)-\tilde{\kappa}_{\rm ideal}(r\Delta t)}{\sigma_r}\right]^2. \quad (28)$$

For quantum Monte Carlo data the assumption of Gaussian distributed errors is often adequate (see Sec. IV A), but the assumption of independent errors is usually very poor. Therefore rather than Eq. (28), we use the definition of χ^2 given by Eq. (26) to calculate the likelihood function, Eq. (25).

The prior knowledge about $\kappa(\omega)$ is that it is a positive and additive distribution. The appropriate prior distribution for this case is the entropic form [52],

$$P[\kappa(\omega)|I]\propto\exp(\alpha S), \quad (29)$$

where S is the generalized Shannon-Jaynes entropy,

$$S=\int d\omega\left[\kappa(\omega)-m(\omega)-\kappa(\omega)\ln\frac{\kappa(\omega)}{m(\omega)}\right], \quad (30)$$

and α is a parameter. The function $m(\omega)$ in Eq. (30) is the default model, i.e., the initial model assumed for $\kappa(\omega)$. Our results are calculated from the Bayesian procedure suggested by Bryan [53]. In this approach the optimal solution to Eq. (23) is given by the average over the posterior probability $P[\alpha|\tilde{\kappa}(t),m(\omega)]$:

$$\kappa_{\rm opt}(\omega)=\int d\alpha P[\alpha|\tilde{\kappa}(t),m(\omega)]\kappa_\alpha(\omega). \quad (31)$$

$\kappa_{\rm opt}(\omega)$ is referred to as the maximum entropy reconstruction, or image. The posterior probability function $P[\alpha|\tilde{\kappa}(t),m(\omega)]$ is found by using Bayes's theorem and making a functional integration [53,54]. $\kappa_\alpha(\omega)$ is the image that maximizes $\alpha S-\chi^2/2$ for a given, fixed α. Note that χ^2 is also an implicit function of α, via $\tilde{\kappa}_{\rm ideal}(t)$. In this work, we take the flat model for $m(\omega)$, i.e., $m(\omega)=$const.

Our Monte Carlo simulation described in Sec. II gives us a single value of $\tilde{\kappa}(r\Delta t)$ for each discrete time $r\Delta t$. In order to gather the statistics for the covariance matrix C we perform about $M=50$ independent simulations with different random number seeds. In each simulation we store $\tilde{\kappa}(r\Delta t)$ for each r. We accumulate the M statistically independent measurements. By the central limit theorem the sample variance of these measurements becomes a measure of the actual variance of measurements as their distribution becomes Gaussian. The relative statistical error, $C_{rr}/\langle\tilde{\kappa}(r\Delta t)\rangle$, resulting from the Monte Carlo simulation is about 0.5%, depending on the imaginary time t and the parameter p of the Monte Carlo simulation (see Sec. II). For the maximum entropy analysis we used about 60 data points $r\Delta t$ along t. For the harmonic oscillator application we performed $N=400$ DMC time steps using the discrete time step $\Delta t=0.012(\hbar/E_h)$ and use only every fifth Monte Carlo data point for the maximum entropy analysis. The maximal value of t is here $t_{\rm max}=3.6(\hbar/E_h)$. Figure 2 demonstrates that the signal $\tilde{\kappa}(t)$ has decayed to a value close to zero for $t_{\rm max}=3.6(\hbar/E_h)$. For the Morse oscillator application we performed $N=3000$ DMC time steps, using the discrete time step $\Delta t=0.002(\hbar/E_h)$ and use only every fortieth Monte Carlo data point for the maximum entropy analysis: here $t_{\rm max}=4.8(\hbar/E_h)$. Since we do not use every Monte Carlo data point, the data input to the maximum entropy analysis are nearly independent. This can be seen if we analyze the covariance matrix C. Aspects concerning the Gaussian sta-

tistics of the Monte Carlo data are discussed at the end of Sec. IV A for the harmonic oscillator application.

Our initial attempts to perform the reconstruction by the regularized inverse Laplace transform developed by Brianzi *et al.* [37,38] were not able to completely resolve spectra with several peaks. The problem seems to be the smoothness assumption entering the regularization scheme rather than the statistical quality of the Monte Carlo data. All final analysis presented in Sec. IV have therefore been performed with the maximum entropy method.

IV. APPLICATIONS

We present an application to the harmonic oscillator (Sec. IV A) and to several Morse oscillators (Sec. IV B). These model applications are ideal for benchmarking our method since the numerical results can be compared with exact analytical solutions. The general Monte Carlo formalism described in Sec. II does impose two restrictions on the trial wave function: The trial wave function has to be nodeless and close to the exact ground state wave function. We use the exact ground state wave function of the harmonic oscillator for our first simulations. Later on in Sec. IV A we present simulations using nonexact ground state wave functions, because in many realistic cases we do not know the exact ground state wave function of the system. In Sec. IV B the method is applied to four Morse oscillators. The harmonic oscillator can be considered as a limiting case of the Morse oscillator where the anharmonicity goes to zero. Realistic molecular systems will generally be anharmonic, so the Morse oscillator is an important test case.

A. Harmonic oscillator

As a first simple example of the Laplace transform method we chose a one dimensional harmonic oscillator. All physical quantities are expressed in atomic units. With mass set equal to $1.0m_e$, the Hamiltonian is given by

$$H=(\hat{a}^{+}\hat{a}+\tfrac{1}{2}), \tag{32}$$

where $\hat{a}^{+}$ and $\hat{a}$ are the raising and lowering operators, respectively. The trial wave function, ψ_T, is chosen to be the exact ground state wave function,

$$\psi_0=\left(\frac{1}{\pi}\right)^{1/4}\exp\left(-\frac{1}{2}x^2\right), \tag{33}$$

and the reference energy $E_{\rm ref}$ is chosen to be the exact ground state energy, $E_0=0.5E_h$. We employ the projection operator

$$A=\hat{x}=\sqrt{\tfrac{1}{2}}(\hat{a}^{+}+\hat{a}), \tag{34}$$

because this operator causes transitions to the first excited state only. The fact that $\hat{x}$ causes transitions to only the first excited eigenstate of the harmonic oscillator motivates the name ''projector'' introduced in Sec. II. The simulation then gives us the energy difference between the ground state level and the first excited state level. This model is a useful test because we can determine $\kappa(\omega)$ and $\tilde{\kappa}(t)$ in this case analytically. Thus,

$$\kappa(\omega)=\tfrac{1}{2}\delta(E_0-E_1+\omega), \tag{35}$$

where $E_0=\frac{1}{2}E_h$ and $E_1=\frac{3}{2}E_h$ are the first eigenenergies of the harmonic oscillator and

$$\tilde{\kappa}(t)=\tfrac{1}{2}\exp(-t). \tag{36}$$

Our simulation should therefore exhibit a single exponential decay, with amplitude 0.5 for $t=0(\hbar/E_h)$ and with a time constant equal to $1.0(E_h/\hbar)$. The maximum entropy analysis should result in a peak at $E_1-E_0=1.0E_h$.

The only systematic error that might occur in the simulation is a DMC time step error. Therefore we checked the time step Δt quite carefully and found a time step of $\Delta t=0.012\hbar/E_h$ to be appropriate. We averaged $p=10^5$ DMC walks for each determination of $\tilde{\kappa}(t)$. We used a quite large skip parameter, $l=100$, to ensure statistical independence of the configurations used as DMC starting points, and performed $N=400$ DMC time steps. The relative statistical uncertainty of each $\tilde{\kappa}(r\Delta t)$ fluctuates along the imaginary time axis t but is always less than 0.5%. This statistical uncertainty stems from the Monte Carlo simulation and can be in principle reduced arbitrarily. The error reduction scales with the square root of the number of samples M. We performed about $M=50$ independent Monte Carlo simulations (each with $p=10^5$ DMC walks), giving us M different samples of $\tilde{\kappa}^{(j)}(r\Delta t)$, $j=1,\ldots,M$, for each $r\Delta t$. We calculate the mean,

$$\langle\tilde{\kappa}(r\Delta t)\rangle=\frac{1}{M}\sum_{j=1}^{M}\tilde{\kappa}^{(j)}(r\Delta t), \tag{37}$$

for each discrete time, $r\Delta t$, and the root-mean-square error,

$$\sigma_r=\sqrt{\frac{\langle[\tilde{\kappa}(r\Delta t)]^2\rangle-[\langle\tilde{\kappa}(r\Delta t)\rangle]^2}{M}}. \tag{38}$$

$\langle\tilde{\kappa}(r\Delta t)\rangle$ given by Eq. (37) and σ_r given by Eq. (38) are our input data for the maximum entropy analysis. For this we use only about 60 regularly distributed data points along t, as described in Sec. III. We checked that these data obey Gaussian statistics (see the end of this section).

Figure 2 shows the simulated exponential decay for $\Delta t=0.012(\hbar/E_h)$. Also shown are two curves for larger time steps. It is evident that larger time steps than $\Delta t=0.012(\hbar/E_h)$ result in an incorrect decay. Smaller time steps do not change the exponential decay and are not shown in Fig. 2. The calculated analytical exponential decay is not shown. It coincides with the simulated decay for $\Delta t=0.012(\hbar/E_h)$. The application of the maximum entropy analysis then results in the spectrum shown in Fig. 3.

We first discuss the simulation using the projector $\hat{x}$. We observe a peak with the mean lying at $\omega_{\rm peak}\approx 1(E_h/\hbar)$. The integral under the peak gives us the prefactor of the exponential decay, namely, $I_{\rm peak}\approx 0.5$. Table I summarizes the exact analytical results and Table II shows the corresponding numerical results. The simulated peak position $\omega_{\rm peak}$ and the integral under the peak $I_{\rm peak}$ agree with the analytical numbers to 1%.

Since we have chosen the projection operator, $A=\hat{x}$, we project only on the first excited wave function

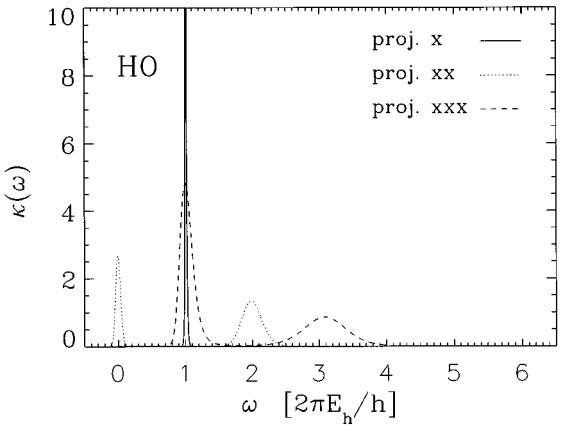

FIG. 3. Harmonic oscillator. The result of the maximum entropy analysis $\kappa(\omega)$ is shown using the exact ground state wave function ψ_0 and the projectors, $\hat{x}$, $\hat{x}^2$, and $\hat{x}^3$.

$$\hat{x}|\psi_0\rangle \propto |\psi_1\rangle. \tag{39}$$

This opens the possibility to check our simulated Monte Carlo data by a least-squares fit. We fit the discrete curve $\tilde{\kappa}(r\Delta t)$ to the analytical form $C\exp(-at)$ where our fit parameters are C and a. Our least-squares result for these two parameters, $C=0.50$ and $a=1.00(E_h/\hbar)$, also agrees perfectly with the exact analytical solution.

Using different projectors like $A=\hat{x}^2,\hat{x}^3,\ldots$ we can project on higher excited eigenstates and therefore get energy differences such as $E_2-E_0, E_3-E_0, \ldots$. The projection operator $A=\hat{x}^2$ results in peaks at $\omega_{\text{peak}}=0(E_h/\hbar)$ and $\omega_{\text{peak}}=2(E_h/\hbar)$ in the $\kappa(\omega)$ spectrum, and the projection operator $A=\hat{x}^3$ results in peaks at $\omega_{\text{peak}}=1(E_h/\hbar)$ and $\omega_{\text{peak}}=3(E_h/\hbar)$. The results of the maximum entropy analysis for these projection operators are also shown in Fig. 3. It is evident that the peaks at higher ω are less pronounced and broader than the peaks at lower ω. The maximum entropy analysis becomes more demanding for simulations using the projectors $\hat{x}^2$ and $\hat{x}^3$ than for simulations using the projector $\hat{x}$, since the spectra are becoming more structured. So, the intensity in each peak is lowered and neighboring peaks might not be separated clearly. Table II summarizes the simulated results for all three projectors, $\hat{x}$, $\hat{x}^2$, and $\hat{x}^3$.

Since we generally do not know the exact ground state wave function for a more complicated system, we also used two nonexact trial wave functions,

TABLE I. Harmonic oscillator. Analytical values for the mean peak position, ω_{peak}, and the integral under the peak, I_{peak}, obtained for the exact ground state wave function ψ_0 using the projectors $\hat{x}$, $\hat{x}^2$, and $\hat{x}^3$. Analytical values for ω_{peak} obtained using the wave functions ψ_{T1} and ψ_{T2} are the same as those obtained with ψ_0. All values are given in atomic units.

	$\hat{x}$	$\hat{x}^2$		$\hat{x}^3$	
ψ_0					
ω_{peak}	1.0	0.0	2 .0	1.0	3.0
I_{peak}	0.5	0.25	0.5	1.125	0.75

TABLE II. Harmonic oscillator. Numerical values for the mean peak positions, ω_{peak}, obtained using the exact ground state wave function ψ_0 and the trial wave functions ψ_{T1} and ψ_{T2}, with the projectors $\hat{x}$, $\hat{x}^2$, and $\hat{x}^3$. The numerical values for the integral under the peak I_{peak} are given for ψ_0 only. All values are given in atomic units.

	$\hat{x}$	$\hat{x}^2$		$\hat{x}^3$	
ψ_0					
ω_{peak}	1.011	0.001	2.000	1.043	3.070
I_{peak}	0.499	0.248	0.500	1.162	0.702
ψ_{T1}					
ω_{peak}	1.008	0.009	2.064	1.040	3.149
ψ_{T2}					
ω_{peak}	0.997	0.011	2.132	1.038	3.413

$$\psi_{T1}=N_{T1}\exp(-0.4x^2) \tag{40}$$

and

$$\psi_{T2}=N_{T2}\exp(-0.3x^2), \tag{41}$$

in order to get an idea how the accuracy of the ground state function affects the results. N_{T1} and N_{T2} are normalization constants. These nodeless trial wave functions can be written as an expansion in the exact eigenstates ψ_j of the harmonic oscillator,

$$\psi_{T1,2}=\sum_j c_j\psi_j. \tag{42}$$

The coefficients c_0 and c_2 give the main contributions in the expansion for both trial wave functions: For the trial wave function ψ_{T1} the ground state wave function contributes about 93% and for the trial wave function ψ_{T1} the ground state wave function contributes about 84%. Therefore, as discussed in Sec. II A, we expect more than one peak in the $\kappa(\omega)$ spectrum if we use, e.g., the projector $\hat{x}$. Since these trial wave functions are even functions, the projector $\hat{x}$ should give us peaks only at odd ω, i.e., $\omega=1(E_h/\hbar)$, $\omega=3(E_h/\hbar)$, etc. The peak positions of the main peaks in the spectrum using the other projectors ($\hat{x}^2$, $\hat{x}^3$, . . .) should still be located at $\omega_{\text{peak}}=0(E_h/\hbar),1(E_h/\hbar),\ldots$. Application of a sequence of different projectors therefore still allows the construction of a complete spectrum. The reference energy is chosen to be the trial energy E_{T1} and E_{T2} in the simulations using trial wave functions ψ_{T1} and ψ_{T2}, respectively.

The results for $\kappa(\omega)$ calculated with the trial wave functions given by Eq. (40) and Eq. (41) are shown in Figs. 4(a) and 4(b), respectively. Calculations were made using $A=\hat{x}$, $\hat{x}^2$, and $\hat{x}^3$. The presence of an increasing number of peaks makes the maximum entropy analysis more demanding. The numerical results are given in Table II. Figure 4(a) shows a peak at $\omega_{\text{peak}}\approx 3(E_h/\hbar)$ using the projector $\hat{x}$, which is enhanced by a factor of 100. This peak arises from the fact that the trial wave function ψ_{T1} is contaminated with the second excited eigenfunction. The results from simulations performed with the trial wave function ψ_{T2} are shown in Fig.

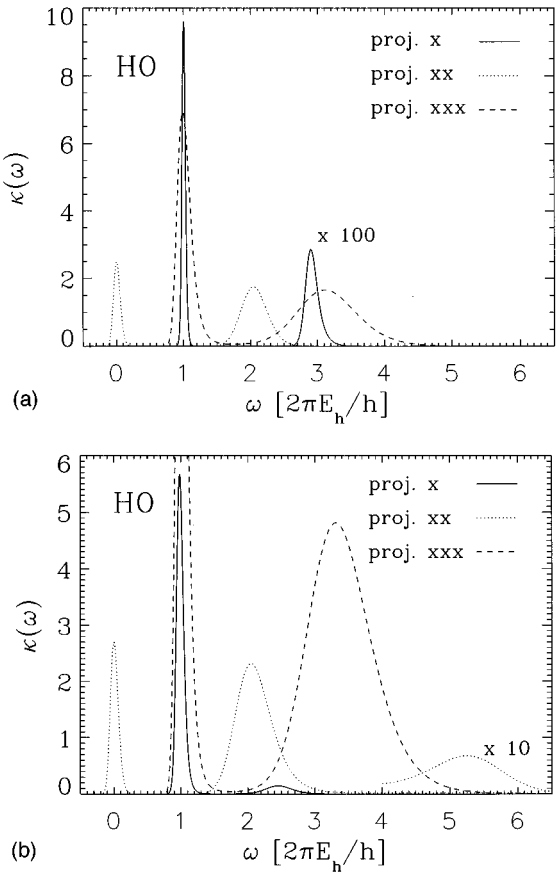

FIG. 4. Harmonic oscillator. The result of the maximum entropy analysis, $\kappa(\omega)$, obtained using the trial wave functions, ψ_{T1} (a) and ψ_{T2} (b), with projectors $\hat{x}$, $\hat{x}^2$, and $\hat{x}^3$. (a) The curve representing the projector $\hat{x}$ (solid line) has a peak at $\omega_{\text{peak}} \approx 1.0(E_h/\hbar)$ and an additional peak at $\omega_{\text{peak}} \approx 3.0(E_h/\hbar)$, which is multiplied here by a factor of 100. (b) The curve representing the projector $\hat{x}^2$ has peaks at $\omega_{\text{peak}} \approx 0.0(E_h/\hbar)$, $\approx 2.0(E_h/\hbar)$ and $\approx 5.5(E_h/\hbar)$. The latter is multiplied by a factor of 10 here.

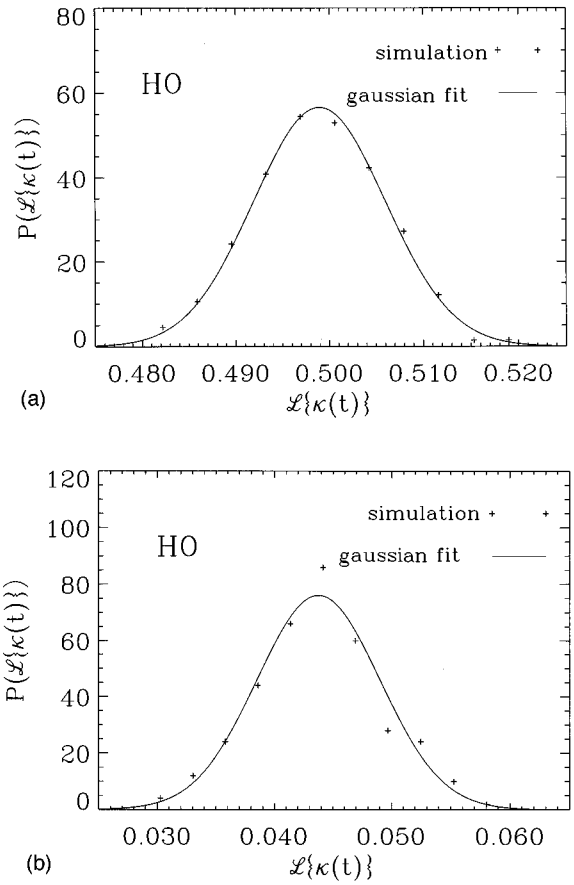

FIG. 5. Harmonic oscillator. The probability distribution of the Monte Carlo data, $\tilde{\kappa}(r\Delta t)$, is shown at the imaginary time values $t=0(\hbar/E_h)$ (a) and $t=2.4(\hbar/E_h)$ (b). These simulated data (symbols), $\tilde{\kappa}^{(j)}(t)$, are binned in histograms. We performed $M=180$ independent simulations using ψ_0 and the projector $\hat{x}$. The Gaussian distribution given by the mean and the variance of the Monte Carlo data is plotted as a solid line for comparison.

4(b). Here we see two additional peaks, which do not occur in Fig. 3. These additional peaks should be theoretically at $\omega_{\text{peak}}=3(E_h/\hbar)$ for $A=\hat{x}$ and at $\omega_{\text{peak}}=4(E_h/\hbar)$ or $\omega_{\text{peak}}=6(E_h/\hbar)$ for $A=\hat{x}^2$. The intensity of these peaks is quite low. The maximum entropy analysis indicates the presence of these additional peaks but is not able to locate them at the correct position. These small additional peaks arise specifically from the nonexact trial wave functions ψ_{T1} and ψ_{T2}, and should not be unduly overemphasized. The reliable information is that there are additional peaks in the spectrum, and not where the *exact* position of these peaks is. A suitable choice of other projection operators can be made to obtain these peaks with higher intensity, and therefore more reliability.

The input for the maximum entropy analysis is the mean given by Eq. (37) and the error given by Eq. (38). The assumption of the analysis requires the input data to obey Gaussian statistics. We used the simulated data from $\psi_T=\psi_0$ with $A=\hat{x}$ and the DMC time step $\Delta t=0.012(\hbar/E_h)$ to check the statistics. Figure 5(a) shows a histogram from many independent Monte Carlo runs of the data $\tilde{\kappa}(r\Delta t)$ for $r=0$ $(M=180)$ and Fig. 5(b) shows a histogram of the data $\tilde{\kappa}(r\Delta t)$ for $r=200$ $(M=180)$. The data for $r=0$ stem from the multidimensional Monte Carlo integration $[t=0(\hbar/E_h)]$. The DMC propagation along the imaginary time t gives us the data for $r=200$, which corresponds to $r\Delta t=2.4(\hbar/E_h)$. The Gaussian distribution corresponding to the mean and the variance of the Monte Carlo data is plotted for comparison in Figs. 5(a) and 5(b). This confirms that our Monte Carlo data definitely obey Gaussian statistics, both for $t=0(\hbar/E_h)$ calculated via a Monte Carlo integration, and for $t>0(\hbar/E_h)$ calculated via DMC.

B. Morse oscillator

The potential of the Morse oscillator is given by

$$V=D_e[1-\exp(-ax)]^2, \tag{43}$$

where D_e is the dissociation energy and a is the range parameter. We restrict ourselves to parameters D_e and a such that the force constant

$$F=2D_e a^2 \tag{44}$$

is equal to 1, as in the harmonic oscillator example. The energy levels of the Morse oscillator are given by

$$E_i=\omega_e(i+\tfrac{1}{2})-x_e(i+\tfrac{1}{2})^2, \tag{45}$$

where

$$\omega_e=a\hbar\sqrt{\frac{2D_e}{m}} \tag{46}$$

and

$$x_e=\frac{(a\hbar)^2}{2m}. \tag{47}$$

The mass of the Morse oscillator is chosen to be equal to $1.0m_e$. The exact ground state wave function can be expressed in terms of D_e and a,

$$\psi_0=N_0 z^{(\omega_e/x_e-1)/2}\exp\left(-\frac{z}{2}\right), \tag{48}$$

where

$$z=\frac{\omega_e}{x_e}\exp(-ax) \tag{49}$$

and N_0 is a normalization constant. The number of bound states k is given by

$$k=\frac{\omega_e}{2x_e}. \tag{50}$$

The projection operators, $A=\hat{x},\hat{x}^2,\ldots,$ no longer project onto only one or two higher eigenstates of the system as for the harmonic oscillator case, but onto the whole manifold.

We use four different Morse oscillators defined in Table 3. They will be referred to as MO1 to MO4. MO1 is very similar to the harmonic oscillator, while MO4 is the most anharmonic oscillator, with only four bound states. In each case we use the exact ground state wave function, the reference energy, $E_{\rm ref}=E_0$, and the projection operator, $A=\hat{x}$. Figure 6 shows the results of the maximum entropy analysis of the imaginary time evolution. We observe two peaks in each spectrum, one at $\omega_{\rm peak}\approx 0(E_h/\hbar)$ and one at $\omega_{\rm peak}\approx 1(E_h/\hbar)$. The peak at $\omega_{\rm peak}\approx 1(E_h/\hbar)$ is progressively shifted to smaller values for the Morse oscillators (relative to the harmonic oscillator value) due to the increasing anharmonicity. Table III demonstrates the excellent agreement between the analytical and the simulated values for the positions of these peaks. The deviation between the simulated and the analytical results is less than 2% for all Morse oscillators. The two peaks in the spectrum for MO4, the most anharmonic oscillator, are not clearly separated (see Fig. 6). The mean of the second peak given in Table III is calculated using $\omega\in[0.35(E_h/\hbar),1.2(E_h/\hbar)]$. Although the maximum entropy analysis does not separate these two peaks clearly, the spectrum does nevertheless show that there are two different peaks in the spectrum, in agreement with analytical predictions. In contrast, MO1 behaves almost like a harmonic oscillator. Thus the projector $\hat{x}$ projects mainly on the first excited eigenstate for $\psi_T=\psi_0$. The peak at

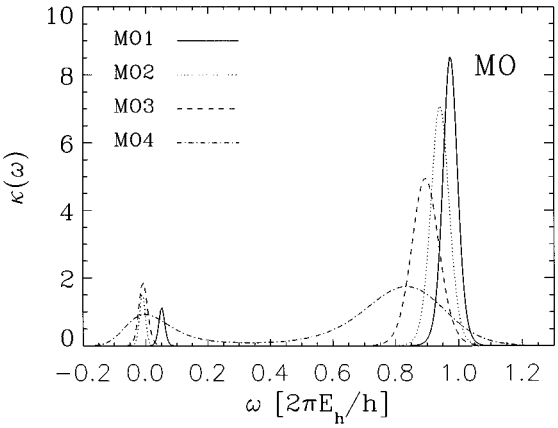

FIG. 6. Morse oscillator. The result of the maximum entropy analysis, $\kappa(\omega)$, obtained for the four Morse oscillators MO1 to MO4 with the projector $\hat{x}$ and the appropriate exact ground state wave function in each case.

$\omega_{\rm peak}\approx 0(E_h/\hbar)$ in the MO1 spectrum, which derives from the anharmonicity, has a very low intensity. The intensity of this peak becomes larger for the oscillators MO2 to MO4, as a result of the increasing anharmonicity. The opposite trend is exhibited by the intensity of the second peak $[\omega_{\rm peak}\approx 1(E_h/\hbar)]$, which becomes smaller going from MO1 to MO4. The absolute maximum of the peak itself does not include any useful information. The physically relevant information is the integral under the peak, and the mean position of the peak. The peak widths depend on the Monte Carlo simulation parameters and on the maximum entropy analysis, namely, on (i) the number of Monte Carlo samples p, (ii) the number of independent Monte Carlo runs M, and (iii) the number of eigenvalues used for the maximum entropy analysis [26].

Typical parameters used in our Monte Carlo implementation are: $\Delta t=0.002(\hbar/E_h)$, $N=3000$, number of samples $p=10^4$, skip parameter $l=100$, and number of independent simulations $M=50$.

V. CONCLUSION

We have presented a method for the calculation of excited state energies of quantum mechanical systems, based on an

TABLE III. Morse oscillator. Parameters a and D_e for the four Morse oscillators MO1 to MO4 (lines 1 and 2), number of bound states k, ground state energy E_0, first excited state energy E_1, and energy difference E_1-E_0 (lines 3 to 6). These are calculated analytically (see text). The position of the peak in the $\kappa(\omega)$ spectrum, $\omega_{\rm peak}$, obtained from the imaginary time simulation is given in line 7. All values are given in atomic units.

	MO1	MO2	MO3	MO4
a	$\frac{1}{5}=0.2$	$\frac{1}{4}=0.25$	$\frac{1}{3}=0.\overline{3}$	$\frac{1}{2}=0.5$
D_e	12.5	8.0	4.5	2.0
k	25	16	9	4
E_0	$\frac{99}{200}$	$\frac{63}{128}$	$\frac{35}{72}$	$\frac{15}{32}$
E_1	$\frac{291}{200}$	$\frac{183}{128}$	$\frac{99}{72}$	$\frac{39}{32}$
E_1-E_0	0.96	0.9375	$0.\overline{8}$	0.75
$\omega_{\rm peak}$	0.974	0.941	0.895	0.782

imaginary time evolution of projected states that is performed by a diffusion Monte Carlo algorithm, followed by a numerical inverse Laplace transform. Our test applications here are restricted to one dimensional problems, but the favorable scaling of the Monte Carlo formalism with the number of degrees of freedom makes this potentially a very useful tool for the treatment of many particle systems. The applications to the harmonic oscillator and to four Morse oscillators of increasing anharmonicity studied here show an excellent agreement with analytical results.

The input needed for this method is the Hamiltonian H, an analytical nodeless trial wave function ψ_T, and an arbitrary reference energy E_{ref}. The reference energy drops out in the final expression and affects only the numerical efficiency of the suggested algorithm. The reference energy should therefore be close to the trial energy E_T. The best trial wave function is the exact ground state wave function. In general a trial wave function close to the exact ground state wave function is a good choice. The simulations presented here for the harmonic oscillator using two nonexact trial wave functions show that the method gives good results even if the trial wave function is not the exact ground state wave function.

The inverse Laplace transform of the imaginary time evolution yields energy differences between the exact ground state and higher excited states of a system. Thus in order to calculate absolute excited state energies, the ground state energy of a system has to be known. One can, for example, perform a standard DMC calculation, which gives the exact ground state energy and a representation of the ground state wave function in the form of a histogram. The information on the ground state wave function provided by the standard DMC calculation could also be used for the construction of the trial wave function needed for the present method. If particular symmetries are present in the system under investigation or if the construction of good approximations to excited state wave functions is possible, the present method could be combined with a fixed node approach. Exploitation of symmetries could be used for the efficient calculation of specific subsets of the complete spectrum. In principle a reweighting algorithm similar to the sidewalk technique employed for the calculation of the expectation values [45] could be used to correct for deficiences of the trial wave function.

McMahon and Whaley [44] used the presented technique to investigate the energy transfer in a quantum cluster system, namely, the energy transfer from rotationally excited Cl_2 to the collective modes of Cl_2He_6. The projection operator is identified here with a coupling potential and thus, their basic formula is the linewidth contribution derived from population transfer via golden rule rates.

The inverse Laplace transform was performed here by the maximum entropy method. When there are many peaks in the spectrum, this transformation can become problematic. This is the case if we use projectors such as $\hat{x}^2$ or $\hat{x}^3$ or trial wave functions ψ_T, such that $A|\psi_T\rangle$ is not close to an eigenstate of the system. We can overcome this by making a judicious choice of the projection operators, in the following fashion. We can choose a sequence of suitable projection operators that allows us to extract energy differences step by step. These projection operators can be used simultaneously in a single simulation, since the configurations created for the sampling of the multidimensional integration and for the imaginary time propagation are not affected by the projection operator. Therefore the computational effort does not increase significantly by using several projection operators simultaneously. Then we can construct a set of spectra that can be compiled to constitute a complete spectrum characteristic for the system of interest. We expect to be able to use these projection operators efficiently for the calculation of experimentally relevant excited states. A particularly interesting class of projectors are those defined in a space-fixed coordinate system, which opens a path to rotationally excited states.

The experience gained with these first applications now opens the possibility to study more realistic systems. One possibility would be the treatment of van der Waals vibrations. The investigation of vibrations of a system like a molecule embedded in a small Ar_n cluster appears to be very interesting. Here we have a vibration of high frequency of the embedded molecule and vibrations of low frequency in the Ar cluster. A model for this realistic test case is a two dimensional system where we use two coupled oscillators with different eigenfrequencies. The projection operator can be chosen to be the coordinate of the first or of the second oscillator. This model application will give us evidence if it is possible to extract vibrations with very different frequencies. The strength of the coupling between the two oscillators can be modified and the influence on the simulation can be checked. This investigation will be the subject of a forthcoming publication.

ACKNOWLEDGMENTS

D.B. is indebted to C. L. Yiu for lectures about probability theory and inspiring discussions. The continued interest and support of J. P. Toennies is gratefully acknowledged. K.B.W. acknowledges support from the NSF Chemistry Division, Grant No. CHE-9318737 and thanks the A.V. Humboldt Foundation for financial support. All calculations were performed on computers purchased through Max-Planck-Society computing grants.

[1] N. C. Handy, Mol. Phys. **61**, 207 (1987).

[2] D. H. Zhang, Q. Wu, J. Z. H. Zhang, M. von Dirke, and Z. Bačić, J. Chem. Phys. **102**, 2315 (1995).

[3] B. L. Hammond, W. A. Lester, Jr., and P. J. Reynolds, *Monte Carlo Methods in Ab Initio Quantum Chemistry* (World Scientific, Singapore, 1994).

[4] R. N. Barnett and K. B. Whaley, J. Chem. Phys. **99**, 9730 (1993).

[5] B. Whaley, Int. Rev. Phys. Chem. **13**, 41 (1994).
[6] D. Blume, M. Lewerenz, F. Huisken, and M. Kaloudis, J. Chem. Phys. **105**, 8666 (1996).
[7] G. Jacucci, *Monte Carlo Methods in Quantum Problems*, edited by M. H. Kalos (Reidel, Dordrecht, 1984).
[8] B. J. Berne and D. Thirumalai, Annu. Rev. Phys. Chem. **37**, 401 (1986).
[9] M. Quack and M. A. Suhm, Chem. Phys. Lett. **183**, 187 (1991).
[10] M. Quack and M. A. Suhm, J. Chem. Phys. **95**, 28 (1991).
[11] D. F. R. Brown, J. K. Gregory, and D. C. Clary, J. Chem. Soc. Faraday Trans. **92**, 11 (1996).
[12] M. Lewerenz, J. Chem. Phys. **104**, 1028 (1996).
[13] M. A. Suhm and R. O. Watts, Phys. Rep. **204**, 293 (1991).
[14] M. Lewerenz and R. O. Watts, Mol. Phys. **81**, 1075 (1994).
[15] P. J. Reynolds, D. M. Ceperley, B. J. Alder, and W. A. Lester, Jr., J. Chem. Phys. **77**, 5593 (1982).
[16] D. F. Coker and R. O. Watts, J. Chem. Phys. **91**, 2513 (1987).
[17] D. F. Coker and R. O. Watts, Mol. Phys. **58**, 1113 (1986).
[18] M. Caffarel, P. Claverie, C. Mijoule, J. Andzelm, and D. R. Salahub, J. Chem. Phys. **90**, 990 (1989).
[19] R. Bianchi, D. Bressanini, P. Cremaschi, and G. Morosi, Chem. Phys. Lett. **184**, 343 (1991).
[20] P. Sandler, V. Buch, and J. Sadlej, J. Chem. Phys. **105**, 10387 (1996).
[21] D. M. Ceperley and B. Bernu, J. Chem. Phys. **89**, 6316 (1988).
[22] B. Bernu, D. M. Ceperley, and W. A. Lester, Jr., J. Chem. Phys. **93**, 552 (1990).
[23] W. R. Brown, W. A. Glauser, and W. A. Lester, Jr., J. Chem. Phys. **103**, 9721 (1995).
[24] M. Caffarel and P. Claverie, J. Chem. Phys. **88**, 1088 (1988).
[25] M. Caffarel and P. Claverie, J. Chem. Phys. **88**, 1100 (1988).
[26] J. E. Gubernatis, M. Jarrell, R. N. Silver, and D. S. Sivia, Phys. Rev. B **44**, 6011 (1991).
[27] D. Thirumalai and B. J. Berne, J. Chem. Phys. **79**, 5029 (1983).
[28] D. Thirumalai and B. J. Berne, J. Chem. Phys. **81**, 2512 (1984).
[29] D. Thirumalai and B. J. Berne, Comput. Phys. Commun. **63**, 415 (1991).
[30] J. Cao and G. A. Voth, J. Chem. Phys. **104**, 273 (1996).
[31] H. B. Schüttler and D. J. Scalapino, Phys. Rev. Lett. **55**, 1204 (1985).
[32] R. N. Silver, D. S. Sivia, and J. E. Gubernatis, Phys. Rev. B **41**, 2380 (1990).
[33] G. Gallicchio and B. J. Berne, J. Chem. Phys. **101**, 9909 (1994).
[34] J. Aubard, P. Levoir, A. Denis, and P. Claverie, Comput. Chem. **11**, 163 (1987).
[35] W. A. Essah and L. M. Delves, Inverse Prob. **4**, 705 (1988).
[36] C. Cunha and F. Viloche, Math. Comput. **64**, 1193 (1995).
[37] P. Brianzi and M. Frontini, Inverse Prob. **7**, 355 (1991).
[38] P. Brianzi, Inverse Prob. **10**, 55 (1994).
[39] W. H. Press, S. A. Teukolsky, W. T. Vetterling, and B. P. Flannery, *Numerical Recipes in Fortran*, 2nd ed. (Cambridge University Press, Cambridge, 1992).
[40] M. Caffarel and D. M. Ceperley, J. Chem. Phys. **97**, 8415 (1992).
[41] J. Bonča and J. E. Gubernatis, Phys. Rev. E **53**, 6540 (1996).
[42] J. Carlson and R. Schiavilla, Phys. Rev. Lett. **68**, 3682 (1992).
[43] M. Hartmann, F. Mielke, J. P. Toennies, A. Vilesov, and G. Benedek, Phys. Rev. Lett. **76**, 4560 (1996).
[44] M. A. McMahon and K. B. Whaley (unpublished).
[45] R. N. Barnett, P. J. Reynolds, and W. A. Lester, Jr., J. Comput. Phys. **96**, 258 (1991).
[46] N. Metropolis, A. W. Rosenbluth, M. N. Rosenbluth, A. H. Teller, and E. Teller, J. Chem. Phys. **21**, 1087 (1953).
[47] P. J. Reynolds, J. Tobochnik, and H. Gould, Comput. Phys. **4**, 662 (1990).
[48] W. von der Linden, Appl. Phys. A **60**, 155 (1995).
[49] D. S. Sivia, *Data Analysis: A Bayesian Tutorial* (Clarendon Press, Oxford, 1996).
[50] M. Jarrell and J. E. Gubernatis, Phys. Rep. **269**, 133 (1996).
[51] A. Papoulis, *Probability and Statistics* (Prentice-Hall, New York, 1990).
[52] S. F. Gull, *Maximum-Entropy and Bayesian Methods in Science and Engineering*, edited by G. J. Erickson and C. R. Smith (Kluwer Academic, Dordrecht, 1988).
[53] R. K. Bryan, Eur. Biophys. J. **18**, 165 (1990).
[54] S. F. Gull, *Maximum-Entropy and Bayesian Methods*, edited by J. Skilling (Kluwer Academic, Dordrecht, 1989).